Bioactive Materials 40 (2024) 212–226

Contents lists available at ScienceDirect

Bioactive Materials

journal homepage: www.keaipublishing.com/en/journals/bioactive-materials

Poly(*p*-coumaric acid) nanoparticles alleviate temporomandibular joint osteoarthritis by inhibiting chondrocyte ferroptosis

Jiaxin Guo [a,b,1], Kai Su [a,b,1], Liying Wang [c,1], Bingyu Feng [a,b,1], Xinru You [d], Miao Deng [a,b], Wei Seong Toh [e,f], Jun Wu [g,h,***], Bin Cheng [a,b,**], Juan Xia [a,b,*]

[a] *Hospital of Stomatology, Sun Yat-sen University, Guangzhou, 510055, PR China*
[b] *Guangdong Provincial Key Laboratory of Stomatology, Guangzhou, 510055, PR China*
[c] *Department of Hematology, The Seventh Affiliated Hospital, Sun Yat-sen University, Shenzhen, 518107, PR China*
[d] *Center for Nanomedicine and Department of Anesthesiology, Brigham and Women's Hospital, Harvard Medical School, Boston, MA 02115, USA*
[e] *Department of Orthopaedic Surgery, Yong Loo Lin School of Medicine, National University of Singapore, 119228, Singapore*
[f] *Faculty of Dentistry, National University of Singapore, 119085, Singapore*
[g] *Bioscience and Biomedical Engineering Thrust, The Hong Kong University of Science and Technology (Guangzhou), Nansha, Guangzhou, 511455, PR China*
[h] *Division of Life Science, The Hong Kong University of Science and Technology, Hong Kong, China*

ARTICLE INFO

Keywords:
Temporomandibular joint osteoarthritis
Poly(*p*-coumaric acid) nanoparticles
Ferroptosis
Oxidative pressure
Cartilage

ABSTRACT

Oxidative stress and inflammation are key drivers of osteoarthritis (OA) pathogenesis and disease progression. Herein we report the synthesis of poly(*p*-coumaric) nanoparticles (PCA NPs) from *p*-courmaic acid (*p*-CA), a naturally occurring phytophenolic acid, to be a multifunctional and drug-free therapeutic for temporomandibular joint osteoarthritis (TMJOA). Compared to hyaluronic acid (HA) that is clinically given as viscosupplementation, PCA NPs exhibited long-term efficacy, superior anti-oxidant and anti-inflammatory properties in alleviating TMJOA and repairing the TMJ cartilage and subchondral bone in a rat model of TMJOA. Notably, TMJ repair mediated by PCA NPs could be attributed to their anti-oxidant and anti-inflammatory properties in enhancing cell proliferation and matrix synthesis, while reducing inflammation, oxidative stress, matrix degradation, and chondrocyte ferroptosis. Overall, our study demonstrates a multifunctional nanoparticle, synthesized from natural *p*-coumaric acid, that is stable and possess potent antioxidant, anti-inflammatory properties and ferroptosis inhibition, beneficial for treatment of TMJOA.

1. Introduction

As one of the most devastating chronic diseases, osteoarthritis (OA) affects 7 % of the global population and imposes a weighty pecuniary bear on families and community [1,2]. The temporomandibular joint (TMJ), which links the mandibular condyle to the temporal articular surface, is among the joints commonly impacted by OA [3]. Similar to OA in other joints, temporomandibular joint osteoarthritis (TMJOA) follows a comparable pathologic trajectory marked by steady deterioration of cartilage, erosion of the subchondral bone, and chronic pain, adversely impacting the lives of those affected [4].

In recent years, although TMJOA drug treatment has achieved certain research results, affording a preliminary main for the progress of anti-inflammatory drugs [5,6], the intricate etiology and distinct physiological construction of TMJOA still make effective prevention and treatment difficult [4,7]. Previous studies reported oxidative stress and inflammation as key mediators of OA, having a promotive correlation with the disease pathogenesis and progression. During joint inflammation, there is a disruption in intracellular redox equilibrium and a rise in reactive oxygen species (ROS), which function as signaling mediators. This exacerbates the evolution of TMJOA by intensifying damage to chondrocytes, hindering the formation of the extracellular matrix

Peer review under responsibility of KeAi Communications Co., Ltd.
* Corresponding author.
** Corresponding author.
*** Corresponding author. Bioscience and Biomedical Engineering Thrust, The Hong Kong University of Science and Technology (Guangzhou), Nansha, Guangzhou, 511455, PR China.
E-mail addresses: junwuhkust@ust.hk (J. Wu), chengbin@mail.sysu.edu.cn (B. Cheng), xiajuan@mail.sysu.edu.cn (J. Xia).
[1] The authors contributed equally to this work.

https://doi.org/10.1016/j.bioactmat.2024.06.007
Received 28 March 2024; Received in revised form 3 June 2024; Accepted 3 June 2024

(ECM), and activating matrix metalloproteinases (MMPs), which directly break down ECM components [8,9]. The main indicators of OA-related cartilage deterioration are the death of chondrocytes and the breakdown of cartilage matrix [10]. As the sole cell type in articular cartilage, chondrocytes maintain cartilage equilibrium by generating and releasing various cytokines and fulfilling the functional requirements of the cartilage matrix [11].

Previous research has mainly focused on autophagy and apoptosis in TMJOA-related chondrocyte death [12]. However, recent research has revealed a significant role of ferroptosis in OA [13,14]. Ferroptosis, a type of cell death that depends on iron and characterized by the accumulation of lipid peroxides and ROS, is increasingly implicated in the pathogenesis of several diseases, including OA [15,16]. Under inflammation and iron overload condition, chondrocytes underwent ferroptosis, with lipid peroxidation, oxidative stress, excessive matrix degradation over matrix synthesis, perturbing the overall matrix homeostasis, leading to cartilage degeneration and OA development [8,17,18]. Thus, reducing inflammation and oxidative pressure to prevent chondrocytes from undergoing ferroptosis may be effective therapeutic strategies for TMJOA. On this note, numerous antioxidants such as curcumin and resveratrol have been explored for treatment of TMJOA. However, their short half-life, poor water solubility, and unsustainable efficacy restrict their clinical utilization [19,20].

p-Coumaric acid (*p*-CA), a naturally occurring phytophenolic acid present in numerous fruits and plants, has been recognized for its benefits in various human health conditions. As a potent antioxidant that reduces oxidative pressure and inflammatory responses, *p*-CA has exhibited therapeutic potential in various disease models, such as tumors, diabetic nephropathy, and plump liver disease, demonstrating its broad application potential [21,22]. For instance, *p*-CA improved impaired glucose tolerance associated with oxidative pressure, apoptosis, and inflammation while inhibiting neuronal cell death in the hippocampus of diabetic rats [23]. Moreover, *p*-CA protects against plump liver disease by reinforcing plump acid oxidation, decreasing oxidative pressure, and decreasing fat synthesis [24]. Recent study also showed that in an *in vitro* setting using rat chondrocytes, *p*-CA effectively diminished inflammation and cellular senescence induced by interleukin (IL)-1β [25]. These observations underscore the therapeutic potential of *p*-CA in managing TMJOA. However, the delivery of *p*-CA is presently hampered by issues such as the lack of appropriate delivery system, release kinetics and stability [26]. The bioavailability of *p*-CA is also restricted by its limited aqueous solubility and unfavorable pharmacokinetics, necessitating the exploration of innovative strategies to enhance its efficacy.

In previous studies, we constructed a library of polymers derived from various phenolic acids, such as salicylic acid, ferulic acid-based polymers, ursolic acid and *p*-CA, and demonstrated their promising potential for disease treatment [27–30]. Based on this foundation, we identified poly(*p*-coumaric acid) nanoparticles (PCA NPs), which are biocompatible and have notable antioxidant and anti-inflammatory effects, for potential treatment of TMJOA. In this study, we used monosodium iodoacetate (MIA) which has been used to induce OA-like lesions in rat TMJs. Here, we assessed the effects of intra-articular injections of PCA NPs in a rat model of TMJOA, and further delved into the molecular mechanisms by which PCA NPs mediated matrix restoration in TMJ repair and regeneration. And we found that PCA NPs could effectively mitigate TMJOA progression by inhibiting inflammation, oxidative stress, matrix degradation, and ferroptosis, while enhancing cell proliferation and restoring matrix synthesis. Importantly, our findings have demonstrated the therapeutic efficacy of PCA NPs in alleviating TMJOA, by targeting ferroptosis in addition to inflammation and oxidative stress, providing new perspectives in TMJ repair (Scheme 1).

2. Experimental section

2.1. Preparation and characterization of PCA NPs

The PCA polymer was synthedimensiond using natural *p*-CA as a monomer, employing a swift solution polycondensation technique as previously described [30]. The construction of the PCA polymer was confirmed through various analyses, comprising ^{1}H-nuclear MRS (^{1}H NMR; Bruker, Germany), FT-IR; (Thermo, USA), and ultraviolet (UV; Bruker, Germany) spectroscopy. Whereafter, the synthedimensiond PCA polymer was executed into NPs using a nanosedimention technique. Briefly, after dissolving both PCA polymer and DSPE-PEG 2k in dimethyl sulfoxide (DMSO) at a concentration of 10 mg/mL, they were mixed in a mass contrast of 2:1. The resulting solution was then added dropwise to ultrapure water under continuous stirring to generate PCA NPs. The NPs solution was suspended in a phosphate-buffered saline (PBS) solution after being concentrated via centrifugation for further use.

The microtopography of the PCA NPs was visualized using a TEM (JEM, Japan). Their dimension and zeta potential were determined through DLS techniques, utilizing equipment from Malvern, UK. To evaluate the PCA NPs' stability, they were dispersed in either plain PBS or PBS replenished with 10 % FBS and monitored over 6 days to measure changes in their dimension and polydispersity index (PDI). Additionally, the antioxidant properties of PCA NPs at varying concentrations were compared with those of hyaluronic acid (HA) using 2,2-Diphenyl-1-picrylhydrazyl (DPPH·) and 2,2′-Azino-bis (3-ethylbenzothiazoline-6-sulfonic acid) (ABTS·) scavenging tests to assess their effectiveness.

2.2. Isolation and culture of rat TMJ condylar chondrocytes

Condylar cartilage from the TMJ of female SD rats, aged 8 weeks,

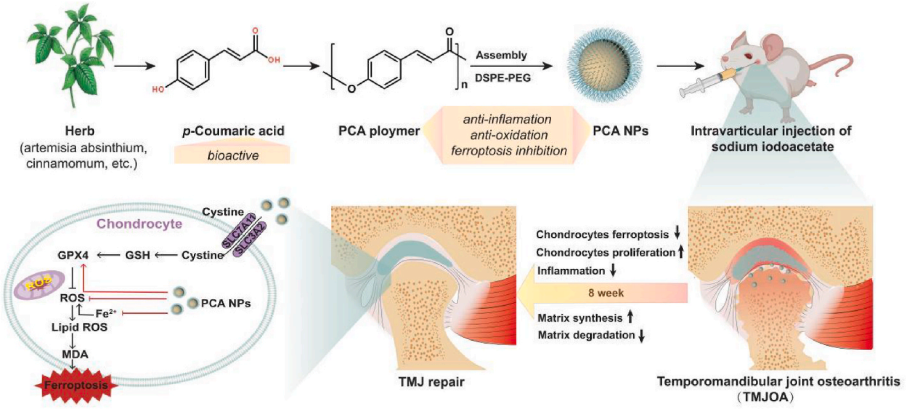

Scheme 1. The mechanism of PCA NPs contribute to the mitigation of TMJOA progression by lowering matrix degradation, increasing proliferation and matrix synthesis, attenuating oxidation and inflammation, and inhibiting chondrocyte ferroptosis.

was meticulously extracted. The cartilage was washed three times in PBS before being subjected to a 4-h digestion at 37 °C using 0.2 % collagenase II (Sigma-Aldrich, USA). The digested tissue was subsequently passed through a 40 μm nylon mesh strainer (Corning, NY, USA) to isolate single cell. These cells were subsequently cultivated in a 5 % CO_2, 37 °C moist environment at a crystal thickness of 20,000 cells/cm^2, using DMEM/F12 medium (HyClone) replenished with 10 % FBS (Gibco, Thermo Fisher Scientific) and 1 % PS (Thermo Fisher Scientific). Upon reaching confluence, chondrocytes were dissociated and subcultured. Passage (P) 2 chondrocytes were used for *in vitro* experiments.

2.3. Cell viability and cellular uptake assays

To assess the potential cytotoxic impacts of PCA NPs on chondrocytes, a CCK-8 (Dojindo, Kumamoto, Japan) was utilized. The chondrocytes were plated in 96-good plates and exposed to varying treatments for durations of 24, 48, or 72 h. Whereafter, 10 μL of CCK-8 solution was introduced into each good. After a 2-h incubation, the OD at 450 nm was quantified employing a microplate reader (Thermo Fisher Scientific, Waltham, MA, USA). Cell viability was further examined employing a live-dead assay kit (Bestbio, China). Following the kit's protocol, a CLSM (Olympus, Japan) was employed to capture pictures. The live cells were identified by their green fluorescence at each good 490 nm excitation, while the dead cells appeared red at 528 nm excitation.

To investigate the uptake of PCA NPs by chondrocytes, coumarin 6 (C6, J&K Scientific) was used to flsorescencely label PCA NPs by nanosedimention. DAPI was added to stain cell nuclei. Cell appearance was then surveied through CLSM; the parameters used were as follows: FITC passage, Ex/Em = 490/520 nm; and DAPI passage, Ex/Em = 364/454 nm.

2.4. qRT-PCR analysis

Total RNA was isolated using an RNA isolation kit (Vazyme, China). The RNA was oppositely recomposed using a oppositely transcription kit (Vazyme, China). RT-PCR was manifestationed using qRT-PCR equipment (Vazyme, China), and Table S1 lists the first nucleotide order used in this investigation. qRT-PCR was utilized to quantify the concentration of OA-specific marker genes, including col2a1, MMP-3, MMP9, MMP13, ADAMTS5, TNF-α , iNOS and PCNA, in chondrocytes. A oppositely transcription kit (Fermentas, Waltham, MA, USA) was utilized to oppositely transcribe the RNA that was withdrawed from the cells into cDNA. The protocol for each qRT-PCR cycle involved: an initial 30 s at 95 °C, subsequent by 40 cycles consisting of 5 s at 95 °C and 34 s at 60 °C.

2.5. Western blot analysis

Protein samples were harvested from each batch of chondrocytes. After centrifuging at 12,000×g for 20 min at 4 °C, the supernatant was mingled into the loading buffer in a 4:1 contrast. This mingle was then heated at 100 °C for 10 min. The proteins were isolated on a 10 % SDS-polyacrylamide gel and subsequently moved to a PVDF membrane (Merck, USA). The membrane was clogged using 5 % BSA for 1 h at ambient temperature. It was then left to incubate overnight at 4 °C with primary antibodies comprising anti-collagen II, anti-MMP13, anti-MMP3, anti-MMP9, anti-iNOS, anti-PCNA, anti-GPX4, anti-ACSL4, anti-SLC7A11, anti-P53 (all at 1:1000, except anti-PCNA at 1:2000 and anti-β actin at 1:5000, sourced from various suppliers). After incubation, the membrane was washed four times for 10 min each in TBST. This was subsequent by a 2-h room temperature incubate with subordinate antibodies (1:5000; Affinity, China) and then three more TBST washes, each lasting 10 min. Blot visualization was accomplished using an ECL kit (GeneGnome XRQ, Syngene, UK).

2.6. Animal experiments

Female SD rats, aged eight weeks and weighing 200–300 g, were obtained from the Laboratory Animal Center of Sun Yat-Sen University. The study's protocol received approval from the Approval Number SYSU-IACUC-2022-000275. These rats were housed under conditions of 25 °C temperature and 50 % humidity. The TMJOA model in the rats was established using MIA injections, as outlined in previous studies [31]. Specifically, each rat received an injection of 0.5 mg MIA (Sigma-Aldrich, USA), solvented in 50 μL PBS, into the bilateral anterosuperior compartment of their TMJs. Following 4 weeks of OA induction, rats in the OA + PCA NP group were treated with 0.5 mg PCA NPs, administered intraarticularly in 50 μL PBS. Similarly, the OA + HA group received intra-articular injections of 0.5 mg HA in 50 μL PBS. Meanwhile, the age-matched naive control remained untreated, and the OA control group received an equivalent cubage of PBS. All animals were euthanized at 2, 4 and 8 weeks post-treatment (Fig. 3A).

2.7. The intra-articular retention effect of PCA NPs in rat TMJ and the distribution of PCA NPs on the surface of cartilage

To evaluate the intra-articular retention effect of NPs, the fluorescence dye (Cy5) was conjugated onto *p*-CA using HOBt and DMAP as coupling reagents and then encapsulated into PCA NPs using nanosedimention method, respectively. After establishing the rat TMJOA model using MIA intra-articular put, 50 μL of free Cy5, Cy5-labeled *p*-CA (*p*-CA-Cy5) and Cy5-labeled PCA NPs (Cy5@PCA NPs) were injected into the TMJOA rats. An *in vivo* imaging system (Lumina XR Series III, PerkinElmer) was used to detect and quantify the fluorescence intensity at different time points after puts. The fluorescence intensity of each joint was determined using the uniform region of interest (ROI) area by Living Image® version 4.4 software. The intensity was set to one at the initial time point, and subsequent days' fluorescence intensity was calculated as the fold change relative to this baseline.

To examine the ultrastructural distribution of PCA NPs on the surface of cartilage, 50 μL of PCA NPs were injected into the rats following OA induction. The condylar cartilage was obtained from the rat after 24 h, then fixed in the 2.5 % glutaraldehyde for 2 h, PBS washed for 3 times, washed three times with PBS, dewatered through a graded ethanol series (30 %, 50 %, 70 %, 80 %, 90 %, 100 %), and freeze-dried. Finally, the surfaces of the prepared cartilage samples were characterized by SEM (Zeiss, Germany).

2.8. Microcomputed tomography (micro-CT) observation

At 2, 4, and 8 weeks post-treatment, the animals were humanely euthanized, and bilateral TMJs were excised through surgery. The isolated TMJ condyles were fixed in 4 % paraformaldehyde for 48 h. For visual examination and documentation of the macroscopic aspects of the TMJ condyles, a micro-CT system (μCT50, Scanco Medical, Switzerland) was employed. The samples were scanned coronally at 70 kV and 114 μA, achieving an effective pixel dimension of 6 μm. Using Mimics software, both sagittal and top views of the condyle were reconstructed. CTvox software was used to evaluate the bone's structural properties. This evaluation included calculating the bone cubage to total tissue cubage volume (BV/TV, %) and trabecular separation (Tb.Sp, mm).

2.9. Histology, immunohistochemical (IHC) and immunofluorescence analyses

Following the micro-CT scanning, the isolated TMJ condyles were decalcified using 0.5 M EDTA (Servicebio, China) for four weeks. The segments were sliced into 4 μm portions and stained with toluidine blue (TB) to assess the deposition of cartilage and with hematoxylin and eosin (HE) to assess overall appearance. The degree of cartilage deterioration in the rat TMJOA model was blindly evaluated using Mankin's scoring

system. The portions were deparaffinized and freezed, remedyed with 3 % hydrogen peroxide for 10 min, and then buried in 0.1 % Triton X-100 for 30 min as preparation for IHC staining. Whereafter, these portions were clogged using 5 % BSA for 1 h. They were then eclosion overnight at 4 °C with main antibodies targeting iNOS, MMP13, Collagen II, GPX4, and ACSL4. Following this, the portions received further incubation with either a goat anti-rabbit IgG (H + L) Fluor488/594 conjugated antibody or a goat anti-rabbit HRP secondary antibody. After DAB staining, the specimens were either scanned using a slice scanner (Leica, Germany) or examined using an Olympus fluorescence microscope (Japan). DAPI (Beyotime, China) was used to counterstain the nuclei before the images were taken. Using ImageJ software, the Collagen II positively stained areas, or MMP13 or iNOS positively stained cells in three random fields were counted at 200× magnification, and expressed as % Collagen II $^{+}$ area, % MMP13^{+} cells, or % iNOS $^{+}$ cells, respectively.

2.10. Condyle RNA extraction, library construction, and sequencing

The animals were euthanized 2, 4, or 8 weeks following treatment, and both TMJs were surgically removed. A portion of the dissected TMJ condyles was collected for transcriptome analysis. Overall RNA extraction, purity quantification and transcriptome analysis were conducted by SequMed BioTechnology, Inc. DESeq R software was used for manifestation analysis. Hierarchical clustering examination was manifestationed to identify patterns of gene manifestation across different groups. R was used for the KEGG pathway enrichment examination and GO enrichment examination based on the hypergeometric distribution.

2.11. Measurement of intracellular iron

Intracellular iron ranks were measured using the FerroOrange flsorescence probe (Dojindo, Japan) was used. Chondrocytes were cultured in a confocal dish and subsequently washed three times with PBS. The FerroOrange reagent was initially solvented in DMSO to achieve a thickness of 1 μM. After incubating for 30 min at 37 °C in the dark, cells were washed three times with PBS and viewed under the fluorescence microscope (Olympus, Tokyo, Japan) with the parameters for Ex/Em = 543/580 nm.

2.12. Mitochondrial appearance and membrane potential staining

Chondrocytes were stained for mitochondrial appearance using MitoTracker Red CMXRos (100 nM, Beyotime, China) at 37 °C for 30 min, followed by nuclear staining with DAPI. Under a fluorescence microscope (LSM 980, Zeiss, Germany), the mitochondria exhibited red fluorescence, while the nuclei appeared blue in the captured pictures. The mitochondria appearance, including the network and branch length, was quantitatively analyzed *via* ImageJ software. In addition, the mitochondrial membrane potential in the chondrocytes was assessed with a JC-1 kit (Beyotime, China). After various treatments, the chondrocytes were placed in JC-1 working solution for 20 min at 37 °C in the dark, subsequent by DAPI staining of the nuclei. Fluorescence pictures taken with a microscope (LSM 980, Zeiss, Germany) displayed red for JC-1 aggregates, green for JC-1 monomer, and blue for nuclei.

2.13. Intracellular ROS and lipid ROS measurements

The concentrations of intracellular ROS and lipid ROS in the cells were quantified employing DCFH-DA (Beyotime, China) and C11 BODIPY581/591 (Thermo Fisher Scientific, USA) flsorescence probes, respectively. The chondrocytes, after being subjected to various treatments, were placed in confocal dishes. They were then treated with either 10 μM DCFH-DA or 10 μM C11 BODIPY581/591 for 30 min at 37 °C in the dark. Fluorescence pictures were captured using an LSM 980 (Zeiss, Germany). Green fluorescence (in which the oxidation state was stimulated at 488 nm) and red fluorescence (in which the oxidation state was not excited at 565 nm) were used to detect the C11 BODIPY581/591 sensor. Flow cytometry (LSRFortessa, BD, USA) analysis was manifestationed, subsequent by quantification of the results.

2.14. MDA, GSH and SOD ranks

The ranks of MDA and GSH, as good as the overall SOD activity in the treated chondrocytes, were determined by employing the Lipid Peroxidation MDA Assay Kit, the GSH and GSSG Assay Kit, and the overall Superoxide Dismutase Assay Kit with WST-8, all sourced from Beyotime, China. These assessments were manifestationed following the manufacturers' provided guidelines.

2.15. Statistical analysis

Total examination of the test information was manifestationed utilizing SPSS version 22.0 (SPSS, USA). The information are displayed as mean ± SEM, and each experiment was replicated independently three times. All experimental information were subjected to normality tests and tests for homogeneity of variance. For determining the total sense in comparisons across multiple groups, ANOVA complemented by Bonferroni correction was utilized. For information plotting, GraphPad Prism 8.0 by GraphPad Software (USA) was applied. A p-value below 0.05 was deemed as declarative of total sense.

3. Results

3.1. Fabrication and characterization of PCA NPs

In our research, natural *p*-CA was chosen as the monomer for synthesizing the bioactive PCA polymer. This synthesis was facilitated by the reaction between the carboxyl and hydroxyl groups in *p*-CA molecules (Fig. S1A). The chemical construction of the resulting PCA polymer was confirmed through ^{1}H-NMR and FT-IR analyses (Figs. S1B and C). Additionally, a redshift in the maximum absorption peak of the PCA polymer, in comparison to the monomer, was surveied in the UV absorption spectra (Fig. S1D), which collectively verified the successful synthesis of the PCA polymer.

Subsequently, the PCA polymer was executed into PCA NPs through a rapid and simple nanosedimention method with the stabilizing agent DSPE-PEG 2k. PCA NPs were characterized by their clarity and stability in liquid form, whereas *p*-CA exhibited challenges in dissolving effectively in water (Fig. S2). A uniform spherical appearance of the PCA NPs was surveied in TEM pictures (Fig. 1A). DLS analysis revealed that the PCA NPs were 118 nm in dimension, had a PDI of 0.26, and had a zeta potential of −18.2 mV (Fig. 1B). Additionally, the PCA NPs demonstrated robust stability, as evidenced by the consistent particle dimension and PDI over 6 days (Fig. 1C, D and E).

Given the good-known antioxidant activities of *p*-CA, we investigated whether PCA NPs retained the antioxidant properties of their monomers through DPPH· and ABTS· scavenging assays. As depicted in Fig. 1F and G, PCA NPs exhibited concentration-dependent DPPH· and ABTS· scavenging abilities, surpassing those of HA at all tested concentrations. Consequently, PCA NPs possess specific antioxidant activities, rendering them advantageous for applications in arthritic disorders.

3.2. The biocompatibility of PCA NPs and their endocytosis by chondrocytes

Evaluating the cytotoxicity of PCA NPs was a vital step prior to examining their effectiveness as ROS scavengers in treating TMJOA, applicable in both *in vitro* and *in vivo* contexts. To assess the effect of PCA NPs on cell viability of condylar chondrocytes, cells were treated with different PCA NP concentrations over 24, 48 and 72 h and assayed using the CCK-8 assay. We observed that cells treated with 75 μg/mL PCA NPs,

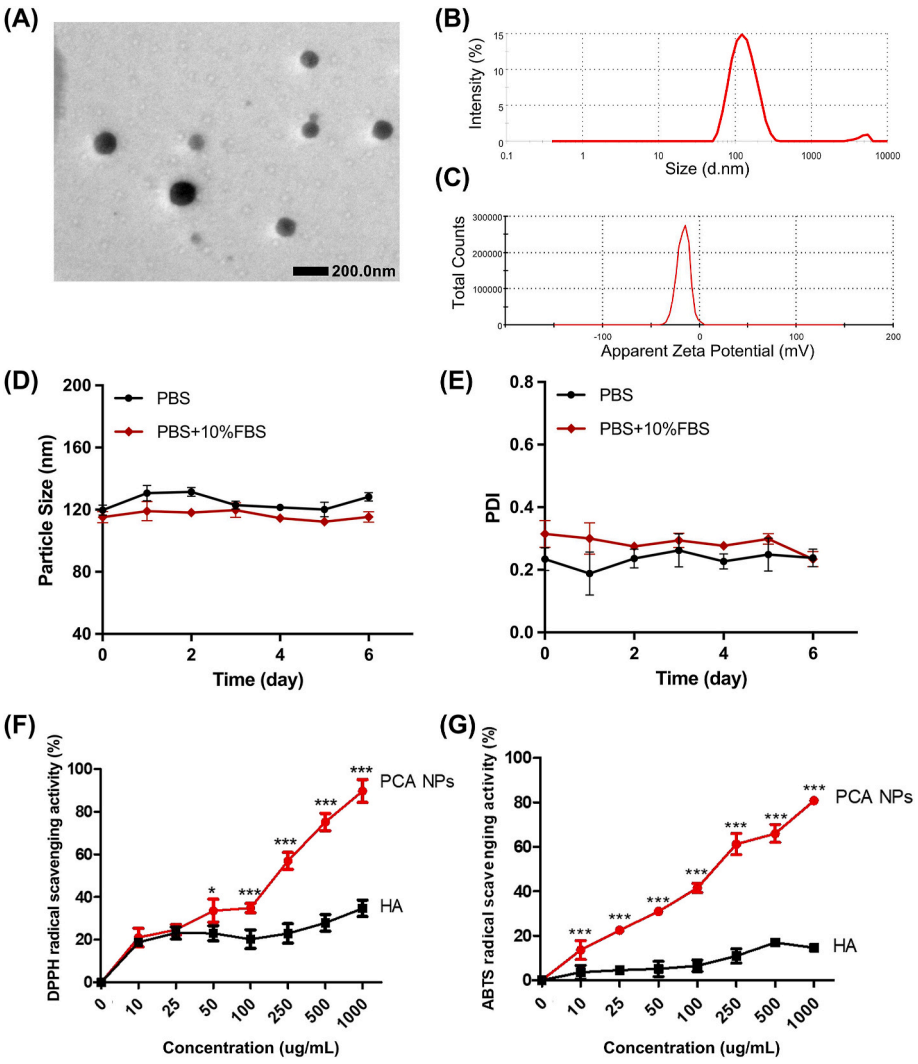

Fig. 1. Characterization of PCA NPs.
(A) Typical TEM photograph showcasing PCA NPs. (B) Dimension distribution of PCA NPs as determined by DLS. (C) Measurement of the zeta potential distribution for PCA NPs. (D and E) Assessment of PCA NPs stability in PBS and PBS supplemented with 10 % FBS. (F and G) Comparative analysis of *in vitro* antioxidant efficacy of PCA NPs against HA. $^{*}P < 0.05$, $^{**}P < 0.01$, $^{***}P < 0.001$ compared to HA.

but not at lower concentrations, had the highest viability at all time points, 24, 48 and 72 h (Fig. S3). There was decline in cell viability with increasing concentrations of PCA NPs higher than 75 μg/mL. Therefore, 75 μg/mL PCA NPs was used in subsequent experiments to treat chondrocytes.

For a more comprehensive analysis of the PCA NPs' cytotoxicity, calcein-AM/PI live/dead cell staining was conducted. The results demonstrated biocompatibility of the PCA NPs, as evidenced by higher number of live cells (green) when cultured with PCA NPs as compared to control, and an almost complete absence of dead cells (red), as shown in Fig. 2B. To learn more about how PCA NPs affect the ability of chondrocytes to survive in an inflammatory environment, we added IL-1β (10 ng/mL) to cultured chondrocytes to construct an *in vitro* chondrocyte OA model [32,33]. Fig. 2A reveals that the cell viability in the group treated with IL-1β experienced a notable decrease following a 24-h incubation period. However, incubation with PCA NPs significantly increased chondrocyte viability and counteracted the negative impact of IL-1β. Next, we used C6-labeled PCA NPs to examine cellular uptake, which was detected by CLSM. C6-labeled PCA NPs were co-cultured with normal medium as control group and medium with IL-1β as inflammation group. Upon incubation alongside chondrocytes for 24 h, the PCA NPs were absorbed by the cells and predominantly distributed throughout the cytoplasm, as depicted in Fig. 2C. In addition, there were no significant alterations in cell appearance with or without IL-1β, which suggests that PCA NPs could be easily uptake by the chondrocytes, and exert its therapeutic effects in an inflammatory joint microenvironment.

3.3. PCA NPs ameliorate the inflammatory effects and matrix degradation induced by IL-1β in vitro

Given that diminishing inflammation and reinstating matrix formation are key requirements for TMJ repair, our study delved deeper into the anti-inflammatory properties and the effects of PCA NPs on chondrocyte catabolism. This exploration was conducted using an *in vitro* cellular OA model stimulated with IL-1β. We first performed immunofluorescence staining of the chondrocytes for Collagen II and MMP13. We observed that while IL-1β stimulation of the chondrocytes reduced their expression of Collagen II and increased their expression of MMP13, PCA NPs were able to counteract these effects of IL-1β by increasing their Collagen II expression while reducing their MMP13 expression (Fig. 2D). By means of western blotting and gene expression analyses of selected anabolic markers (Collagen II and PCNA), and catabolic markers (MMP3, MMP9, MMP13, iNOS, ADAMTS5 and TNFα), we further showed that PCA NP treatment effectively counteracted/reversed the

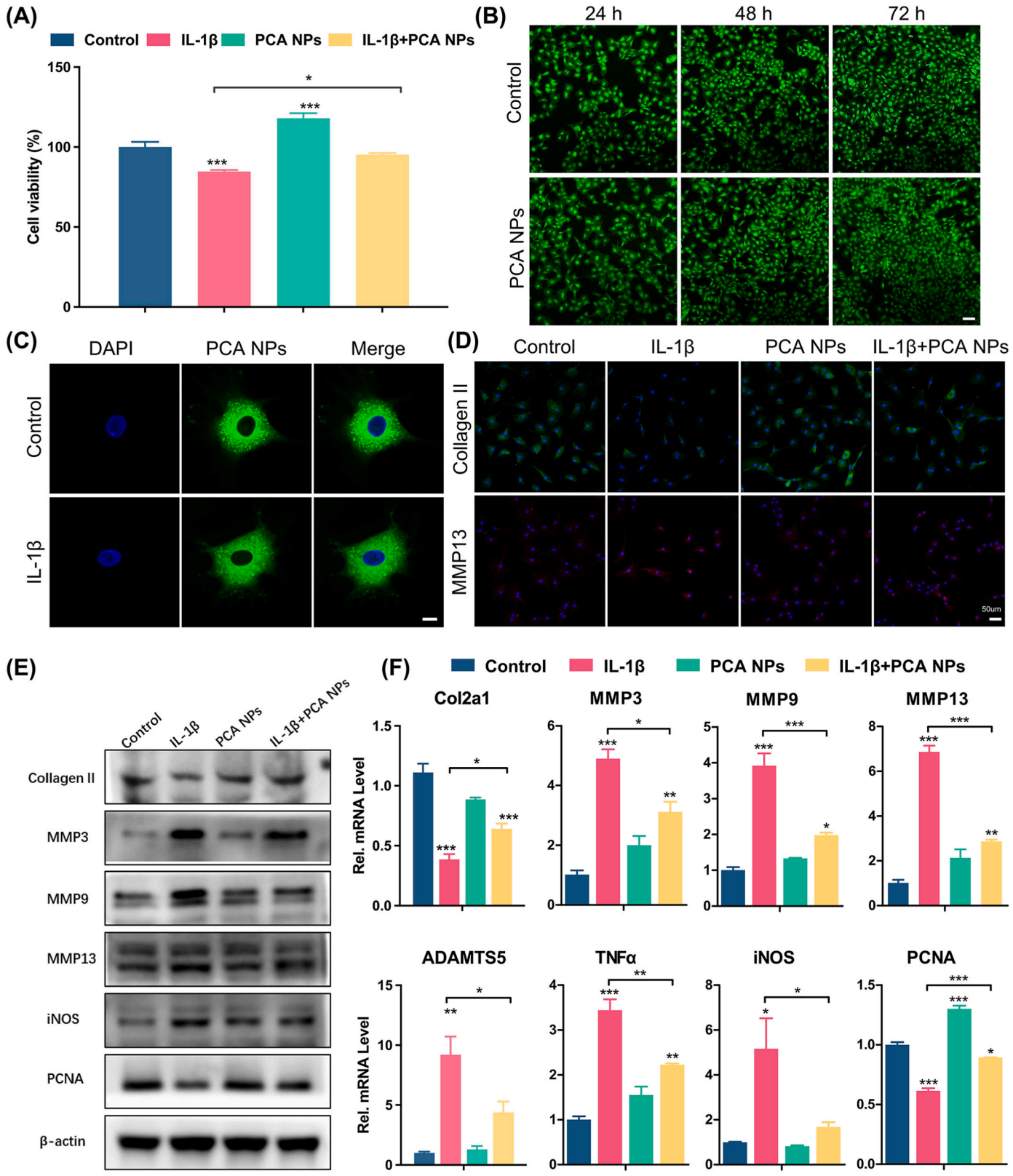

Fig. 2. Chondroprotective effects of PCA NPs on chondrocytes stimulated under IL-1β-induced inflammation *in vitro*.
(A) Effects of PCA NPs on viability of IL-1β-treated chondrocytes. (B) Live/dead staining of chondrocytes treated with 75 μg/mL PCA NPs. Scale bar: 100 μm. (C) Internalization of C6-labbled PCA NPs by chondrocytes, with or without IL-1β stimulation for 24 h. Scale bar: 10 μm. (D) Representative immunofluorescence pictures showing Collagen II and MMP13 in chondrocytes. Scale bar: 50 μm. (E) Western blot analysis of anabolic markers (Collagen II and PCNA), and catabolic markers (MMP3, MMP9, MMP13 and iNOS). (F) Gene expression analysis of anabolic markers (Col2a and PCNA) and catabolic markers (MMP3, MMP9, MMP13, ADAMTS5, TNFα and iNOS). $^{*}P < 0.05$, $^{**}P < 0.01$, and $^{***}P < 0.001$ compared to the control group.

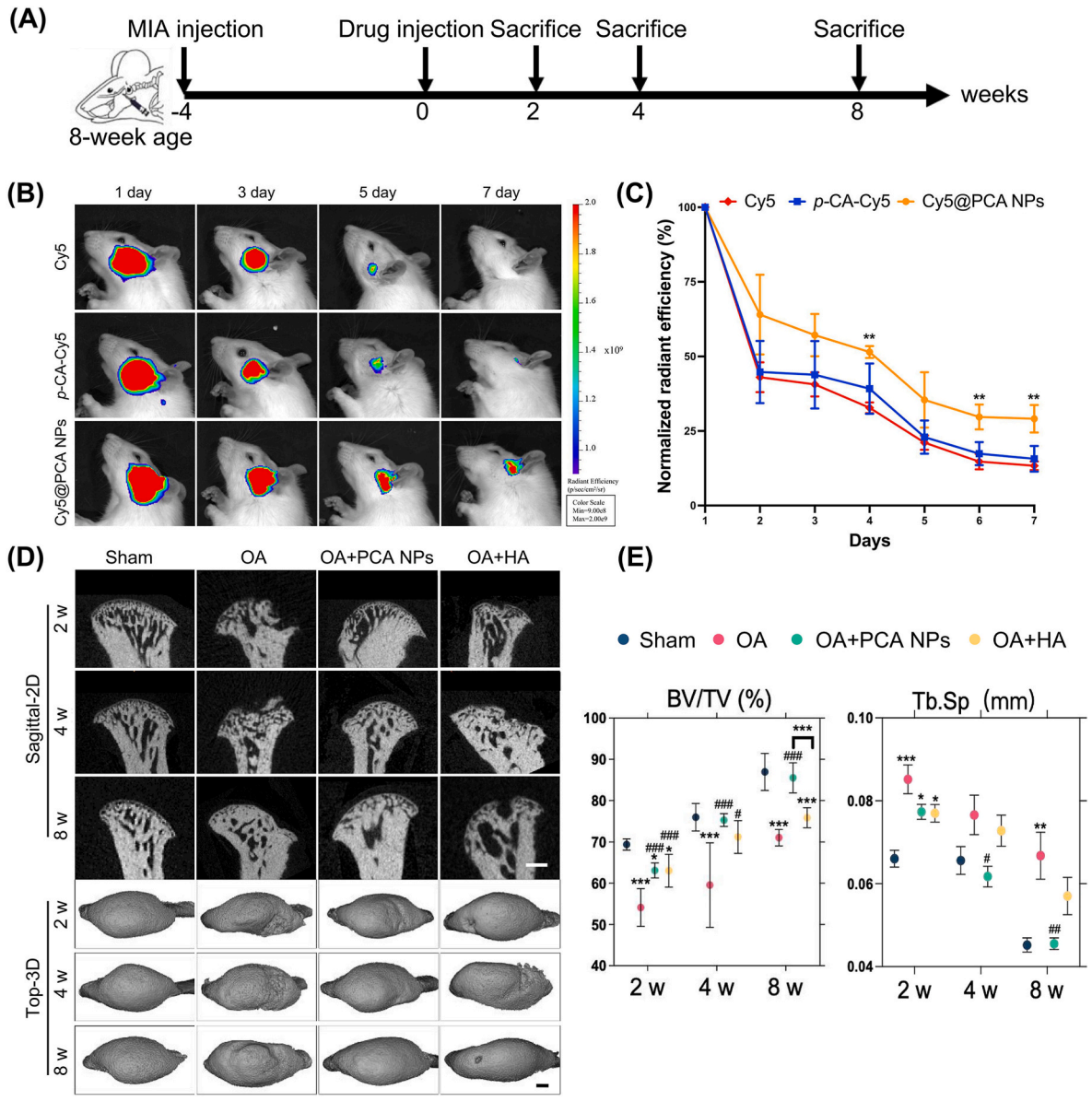

Fig. 3. PCA NPs alleviate subchondral bone destruction and promote TMJ repair in TMJOA.
(A) Depiction of the *in vivo* experimental procedure. (B and C) Representative fluorescence pictures (B) and quantitative analysis of normalized flsorescence radiant efficiency within the rat TMJ (C) at various time points after removing the hair and intra-articular injection of free Cy5, *p*-CA-Cy5 and Cy5@PCA NPs. $^{**}P < 0.01$ compared to the free Cy5 group. (D and E) Rat TMJs were collected for micro-CT examination at intervals of 2, 4, and 8 weeks. (D) Sagittal and top views of the condyles. Scale bar: 500 μm. (E) Analysis of BV/TV and Tb.Sp. $^{*}P < 0.05$, $^{**}P < 0.01$, $^{***}P < 0.001$ compare to the sham rats; $\#P < 0.05$, $\#\#P < 0.01$, $\#\#\#P < 0.001$ in contrast to the OA rats.

effects of IL-1β-induced upregulation of MMP3, MMP9, MMP13, iNOS, ADAMTS5 and TNFα, as well as downregulation of Collagen II and PCNA. These findings demonstrate the potent anti-oxidant and anti-inflammatory properties of PCA NPs in alleviating OA inflammation and oxidative stress. Collectively, our findings show that PCA NPs could restore cartilage matrix homeostasis in TMJOA, by attenuating inflammation, reducing oxidative stress, and inhibiting matrix degradation, while enhancing cell proliferation and augmenting matrix synthesis (Fig. 2E and F).

3.4. PCA NPs demonstrate cartilage-penetrating ability and alleviate TMJ cartilage degeneration in rats

A TMJOA model, induced by MIA, was developed in SD rats to explore the function of PCA NPs in the evolution of TMJOA. In this work, intra-articular injection were administered to three different groups: the OA group received PBS, the OA + PCA NP group received PCA NPs, and the OA + HA group received HA. At 2, 4, or 8 weeks post-injection, the rats were sacrificed. Similar needle pricks were administered to the sham group, but no injections were given (Fig. 3A). Hyaluronic acid (HA) was used as a positive control as it is commonly used as visco-supplementation in joint repair.

To explore the retention effect of PCA NPs, free Cy5, Cy5-labbeled (*p*-CA-Cy5), and Cy5-labbeled PCA NPs (Cy5@PCA NPs) were intra-articularly injected into the TMJ of TMJOA rat, subsequent by serial evaluation for 7 days. As shown in Fig. 3B and C, after a single intra-articular injection, the fluorescence signal in the joints treated with Cy5@PCA NPs was markedly stronger than those injected with Cy5 and *p*-CA-Cy5 at all time points. Besides, the fluorescence signal in rat TMJ in the Cy5 and *p*-CA-Cy5 group exhibited a rapid decline and nearly vanished by the 5th day. However, the Cy5@PCA NPs group still exhibited a visible fluorescence signal and maintained a persistent fluorescence

intensity until the 7th day. These results validated the advantage of PCA NPs in prolonging the retention time within the joint, which suggest that PCA NPs hold promise as an intra-articular drug delivery system for targeting the TMJ cartilage. Furthermore, scanning electron microscopy (SEM) of the rat condylar cartilage after 12 h following intra-articular injection revealed robust adhesion of PCA NPs to the fibrocartilage surface, suggesting that PCA NPs possess the potential to penetrate the cartilage matrix to repair the injured cartilage (Fig. S4).

Parametric analysis and micro-CT imaging were used to assess subchondral bone remodeling. Four weeks after injecting MIA, rats in the OA group exhibited localized collapse of the cartilage surface, subchondral bone degradation and increased marrow cavities (Fig. 3D and

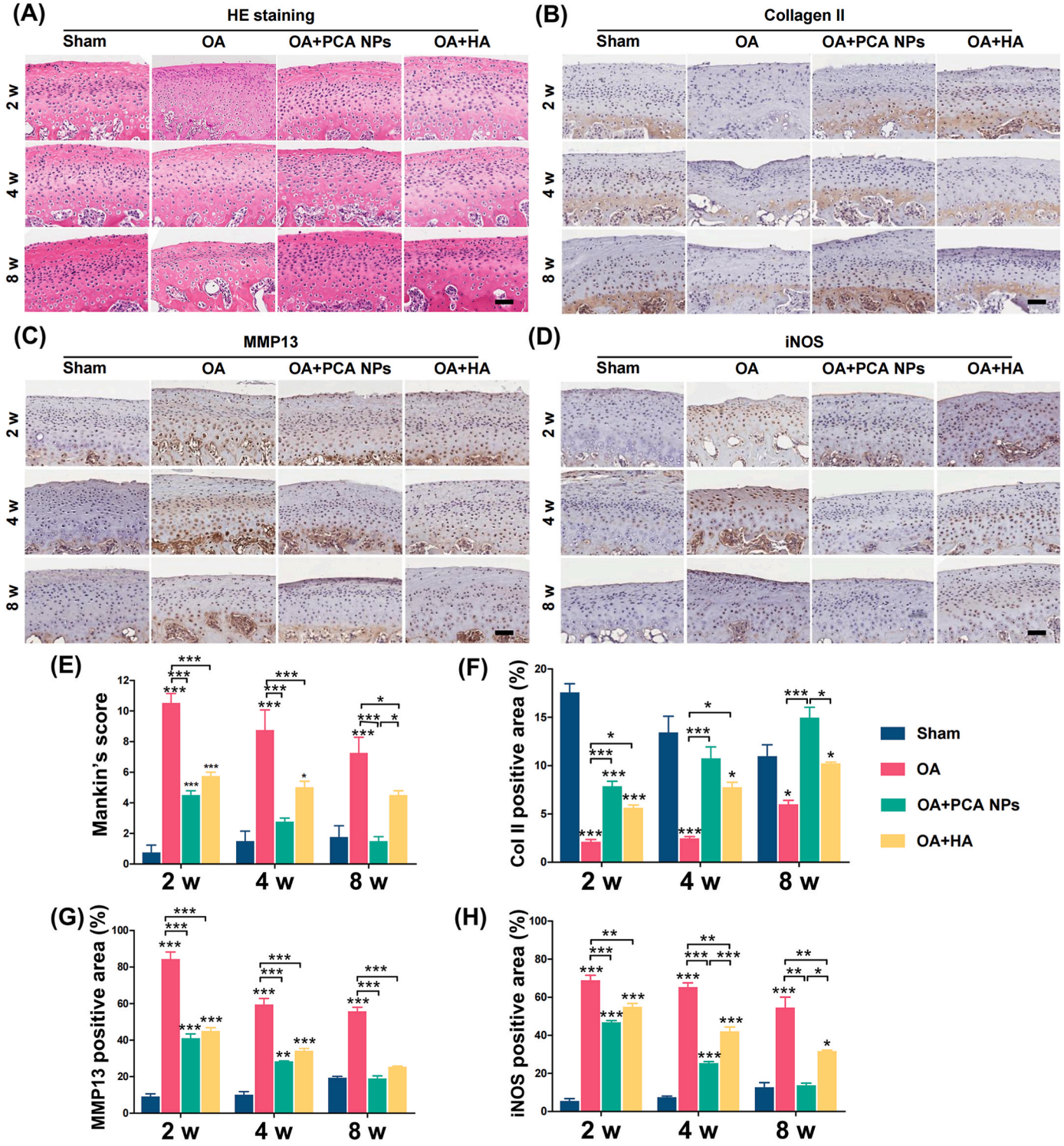

Fig. 4. PCA NPs alleviated condylar cartilage degeneration in TMJOA.
(A–D) Histological staining by (A) hematoxylin and eosin (HE) and immunohistochemical staining for (B) Collagen II, (C) MMP13, and (D) iNOS at 2, 4 and 8 weeks following treatment. Scale bar: 50 μm. (E) Assessment of Mankin's score. (F–H) Quantitative analysis of (F) Collagen II^{+} area, (G) iNOS^{+} cells, and (H) MMP13^{+} cells in the condylar cartilage over 2, 4, and 8 weeks. $^{*}P < 0.05$, $^{**}P < 0.01$, $^{***}P < 0.001$ compared to the sham group at corresponding time points.

E). The OA group exhibited more pronounced degradation of cartilage and subchondral bone in contrast to the sham group. In the PCA NP and HA groups, following two weeks of treatment, bone destruction was still evident, including some damage extending into the deep subchondral bone. However, there was a noticeable partial recovery in the integrity of the bone cortex. Over time, the condylar cartilage bone also continued to recover. After 8 weeks of treatment, subcondylar bone destruction was significantly relieved in the PCA NP group, and the surface cortical smoothness was markedly improved compared to that in the OA group. Conversely, rats in the OA group continued to display significant bone destruction in the condyle, while those in the HA group also demonstrated some degree of bone loss, as illustrated in Fig. 3D. Further quantitative analysis of the bone mineral thickness (BMD) index of the condyle in each group revealed that the OA group presented a reduction in BV/TV and an increase in Tb.Sp. In the OA + PCA NP group, the BV/TV contrasts increased and the Tb.Sp values decreased in the deteriorated subchondral bone, Contrast to the OA group, indicating a significant increase in subchondral bone mass (Fig. 3E). It's important to note that initially, there were no marked differences in BV/TV between the PCA NP and HA groups. However, after an 8-week treatment period, the BV/TV in the PCA NP group was weightyly higher than in the HA collectivity. Thus, while the HA treatment did show some recovery in bone destruction contrast to the OA group, its effectiveness was less pronounced than in the PCA NP treatment group (refer to Fig. 3 D and E).

H&E staining revealed that typical cartilage had a smooth surface and regular cell organization; however, in the OA group, the overall arrangement of cartilage chondrocytes was disorganized. Additionally, TB staining indicated cartilage loss in the OA group. Mankin's scoring system, a widely recognized scoring system for assessing the severity of OA, was used to assess cartilage destruction. The results of our study revealed that the condylar cartilage appearance in both the PCA NPs and HA group showed weighty normalization compared to the OA group at 2, 4, and 8 weeks post-treatment. Additionally, at 4 and 8 weeks post-treatment, the appearance in the PCA NP group did not exhibit a significant difference compared to that in the normal control group. However, at the 8-week mark, the Mankin's score for the PCA NP group was significantly less than in the HA group, aligning with the findings from the micro-CT information (Fig. 4). However, the TMJ cartilage of the OA group had lower ranks of collagen II manifestation, as indicated by the percentage of positive area in the IHC evaluations. However, the

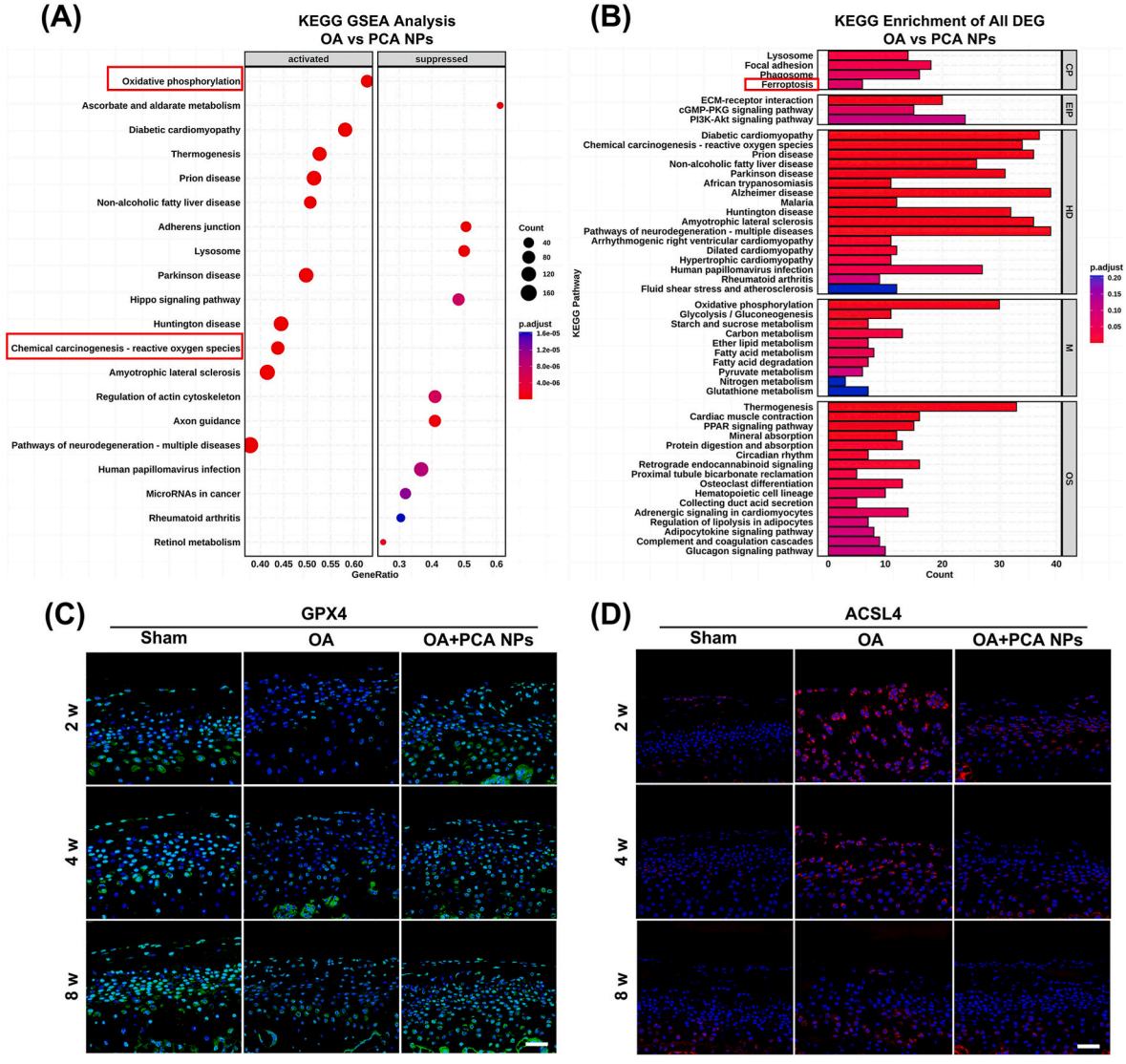

Fig. 5. PCA NPs inhibited chondrocyte ferroptosis in rat TMJOA.
(A and B) Transcriptomic analysis of TMJ condylar cartilage tissue. (A) Results from KEGG GSEA analysis comparing the OA and PCA NPs groups. (B) Results from KEGG enrichment of all DEG analysis comparing the OA and PCA NPs groups. (C and D) Exemplary immunofluorescence staining pictures for GPX4 and ACSL4. Scale bar: 40 μm.

percentage of collagen II-positive areas increased following the intra-articular injection of PCA NPs (Fig. 4B and F). The intra-articular injection of PCA NPs, in contrast to the OA group, counteracted the increased manifestation of MMP13 and iNOS, as shown in Fig. 4C, D, G and H. Taken together, these findings indicated that PCA NPs might prevent cartilage deterioration to halt the progress of osteoarthritis in the rat TMJOA model, which aligns with the outcomes from the *in vitro* experiments, as illustrated in Figs. 3 and 4. Taken together, these findings showed that by blocking articular cartilage breakdown, PCA NP supplementation may delay the evolution of TMJOA.

Our information consistently indicated that PCA NPs possessed excellent joint retention ability, diminished inflammation and promoted comprehensive regeneration of the matrix in both the TMJ condylar cartilage and subchondral bone, thereby averting TMJ degeneration. In summary, these observations imply that PCA NPs reduce tissue damage and promote tissue healing in TMJOA.

3.5. PCA NPs alleviate cartilage degeneration by suppressing ferroptosis

To shed light on the mechanism of action of PCA NPs in TMJOA, we conducted transcriptome sequencing analysis of rat condylar cartilage tissues. GO and KEGG analyses were conducted on genes that exhibited differential manifestation between the OA and the PCA NPs group. According to the KEGG analysis results, PCA NPs intervention in chondrocytes was closely linked to oxidative pressure (Fig. 5A). KEGG enrichment analysis revealed several pathways and processes modulated by PCA NPs. Among all, ferroptosis-related pathways were chosen for further investigation (Fig. 5B).

Next, we investigated whether chondrocyte ferroptosis occurs in rat TMJOA and assessed the effect of PCA NPs on chondrocyte ferroptosis. Key regulatory factors, such as GPX4 crucial for decreasing lipid peroxide toxicity and preserving lipid bilayer homeostasis in cell membranes and ACSL4, involved in synthesizing phospholipids like phosphatidyl ethanolamine and phosphatidyl inositol in negative membranes, were identified using immunofluorescence staining (Fig. 5C and D). Consequently, lower expression of GPX4 and higher expression of ACSL4 were observed in the OA animals compared to the sham animals. Notably, PCA NP treatment was able to reverse the expression of GPX and ACSL4 to levels of the sham animals at 8 weeks post-treatment.

3.6. PCA NPs protect osteoarthritic chondrocytes by attenuating sensitivity to ferroptosis

Next, we manifestationed *in vitro* experiments to confirm our findings and to obtain additional insights into the function of PCA NPs in chondrocyte ferroptosis. We used erastin, a classical ferroptosis inducer, to stimulate chondrocytes and determine the optimal concentration (Fig. S5). The viability of cells stimulated by erastin was significantly suppressed, and the chondrocytes were protected against erastin-induced cell death by PCA NPs, indicating that PCA NPs had a protective effect on the activity of chondrocytes under ferroptotic conditions (Fig. 6A). Additionally, GPX4, ACLS4, SLC7A11 and P53 have been widely studied as ferroptosis markers. In our research, we examined the protein manifestation through western blot analysis and immunofluorescence staining, as illustrated in Fig. 6B and C. Chondrocytes exposed to IL-1β and erastin exhibited a marked elevation in ACSL4 and P53 manifestation, surpassing ranks in the control group, along with a notable reduction in GPX4 and SLC7A11 manifestation. PCA NP treatment effectively reversed these alterations.

Additionally, ferroptosis is distinguished by an excess of iron, which forms the foundation for subsequent adverse occurrences, including the generation of lipid ROS and ROS. As anticipated, after chondrocytes were exposed to erastin, there was a considerable increase in the intensity of orange fluorescence, which represents cellular iron, contrast to that in the control group. In contrast to the erastin-stimulated group, the PCA NP-treated group exhibited a reduced iron overload (Fig. 6D and G). Mitochondrial dysfunction is characterized by an aberrant change in the mitochondrial membrane potential, which is widely acknowledged as a marker of ferroptosis [34,35]. In our study, MitoTracker Red staining and JC-1 staining were performed to investigate the effect of PCA NPs on mitochondrial protection during chondrocyte ferroptosis. As shown in Fig. 6E–G and H, ferroptosis triggered by erastin induced distinctive changes in chondrocytes, such as mitochondrial deformation and shrinkage, as indicated by a reduced or condensed dimension. However, the application of PCA NPs inhibited harmful changes in the appearance of the mitochondria. Conversely, erastin treatment led to the fragmentation of JC-1 aggregates (indicated by red fluorescence intensity) into JC-1 monomer (shown by green fluorescence intensity). This resulted in a noticeable decline in the red/green fluorescence intensity ratio, implying an escalation in mitochondrial damage. Notably, the diminution or loss of mitochondrial membrane potential was partly mitigated following PCA NP administration (Fig. 6F). The findings from both experiments suggest that PCA NPs enhanced the preservation of mitochondrial morphology and membrane potential against damage caused by erastin-induced ferroptosis.

Cellular ROS and lipid ROS are essential for the mechanism of ferroptosis. As depicted in Fig. 7A–D, erastin stimulation of chondrocytes resulted in accumulation of cellular and lipid ROS. PCA NPs effectively reduced the buildup of both cellular ROS and lipid ROS induced by erastin. Additionally, the concentration of MDA, a marker of lipid peroxidation, was evaluated. PCA NP administration mitigated the erastin-induced rise in intracellular MDA levels (Fig. 7E). A hallmark of ferroptosis is the depletion of GSH, an essential intracellular antioxidant. The information showed that erastin exacerbated GSH depletion, while PCA NP treatment lessened GSH consumption, elevating intracellular GSH ranks compared to those in the erastin group (Fig. 7F). Notably, PCA NP treatment also led to an increase in SOD activity, indicating a reduced degree of oxidative pressure compared to the inhibition induced by erastin (Fig. 7G).

In the context of TMJOA, IL-1β, a classic inflammatory factor, was used to establish an inflammatory cell model. Fascinatingly, akin to the effects of erastin, IL-1β stimulation increased the expression of P53 and ACSL4, while concurrently downregulating GPX4 and SLC7A11 manifestation in chondrocytes. This also caused iron overload, mitochondrial malfunction, and lipid peroxidation in chondrocytes, primarily manifesting as the accumulation of cellular and lipid ROS. Moreover, after IL-1β stimulation, MDA ranks increased, and GSH content and SOD activity decreased. Remarkably, PCA NPs reversed the above changes (Fig. S6). These findings suggested that IL-1β could trigger specific changes in chondrocytes related to ferroptosis, implicating the role of ferroptosis in OA pathogenesis and progression.

To summarize, the outcomes of this experiment demonstrate that ferroptosis indeed takes place in a chondrocyte model of TMJOA. PCA NPs protected against the evolution of TMJOA by efficiently blocking the ferroptosis process, as evidenced by their impact on ROS levels, lipid peroxidation, and antioxidant system.

4. Discussion

TMJOA is an major subtype of temporomandibular disorders (TMDs) and mainly characterized by progressive cartilage degradation, subchondral bone erosion and chronic pain. Given that oxidative stress and inflammation are key drivers of OA pathogenesis and progression, we hypothesized that PCA NPs synthesized from *p*-CA, a naturally occurring phytophenolic acid, would exhibit potent anti-oxidant and anti-inflammatory properties to alleviate TMJOA and promote joint repair. Progressive cartilage degradation and subchondral bone changes are the main characteristics of TMJOA and the focus of scholarly attention in recent years. Although there have been deeper discoveries about pathogenic mechanisms involving the cartilage and subchondral bone, such as gene regulation, stem cell differentiation, and pathological cartilage calcification, the exact mechanisms remain to be completely clarified

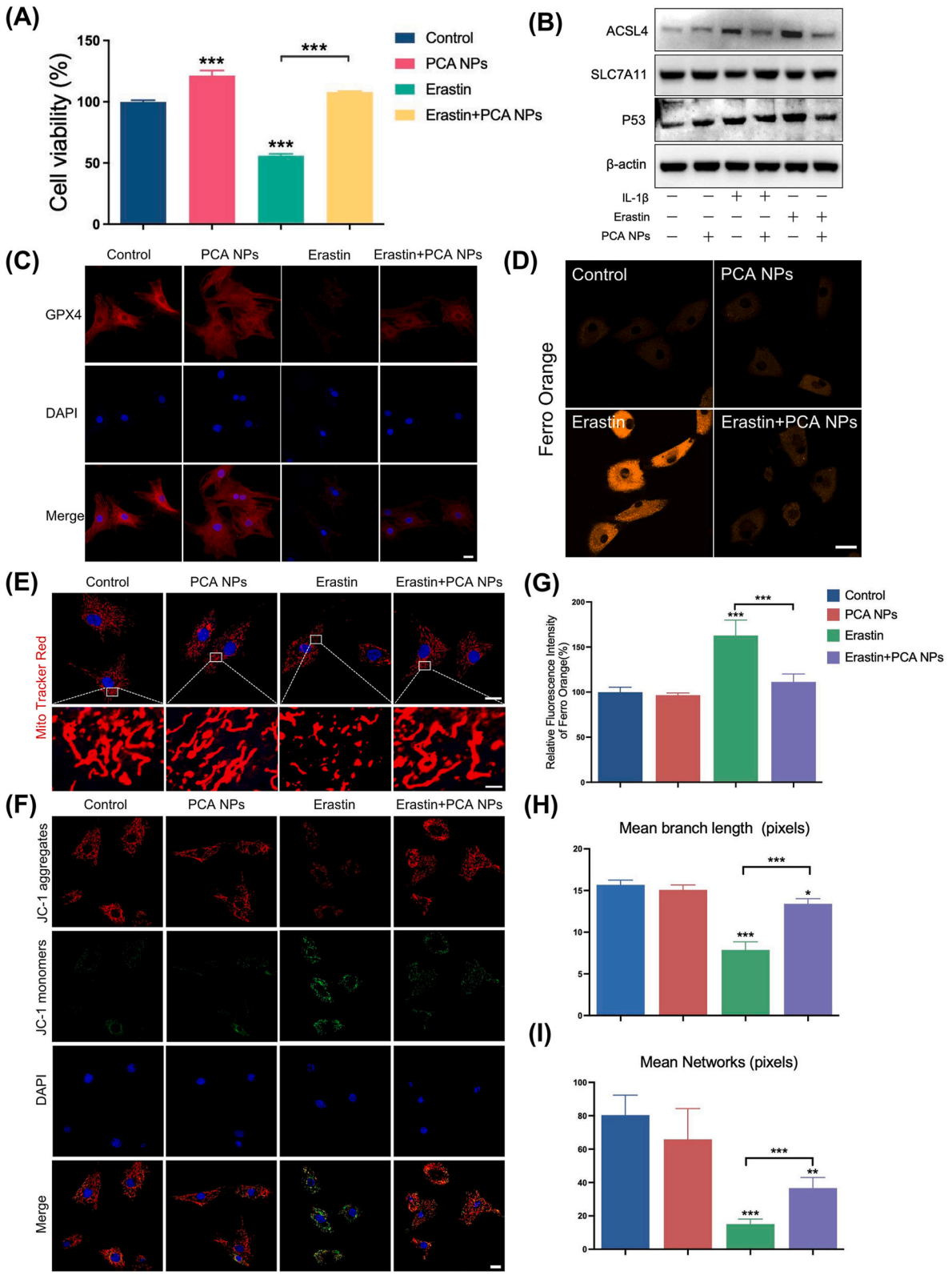

Fig. 6. PCA NPs alleviated Fe^{2+} overload and mitochondrial dysfunction in chondrocytes stimulated with erastin.
(A) Impact of PCA NPs on IL-1β-stimulated chondrocyte activity. (B) Western blotting was used to assess ACLS4, SLC7A11, and P53 protein expression in chondrocytes. (C) Immunofluorescence staining for GPX4 in chondrocytes. Scale bar: 20 μm. (D and G) FerroOrange flsorescence probe staining (D) with its quantitative analysis (G) for Fe^{2+} in chondrocytes. Scale bar: 20 μm. (E, H and I) MitoTracker Red staining (E) along with quantitative evaluations of average mitochondrial branch length (H) and network (I) in chondrocytes. Scale bar: 20 μm. (The enlarge scale bar: 2 μm). (F) JC-1 staining for assessing mitochondrial membrane potential of chondrocytes. Scale bar: 20 μm $^{*}P < 0.05$, $^{**}P < 0.01$, $^{***}P < 0.001$ in comparison to the control group.

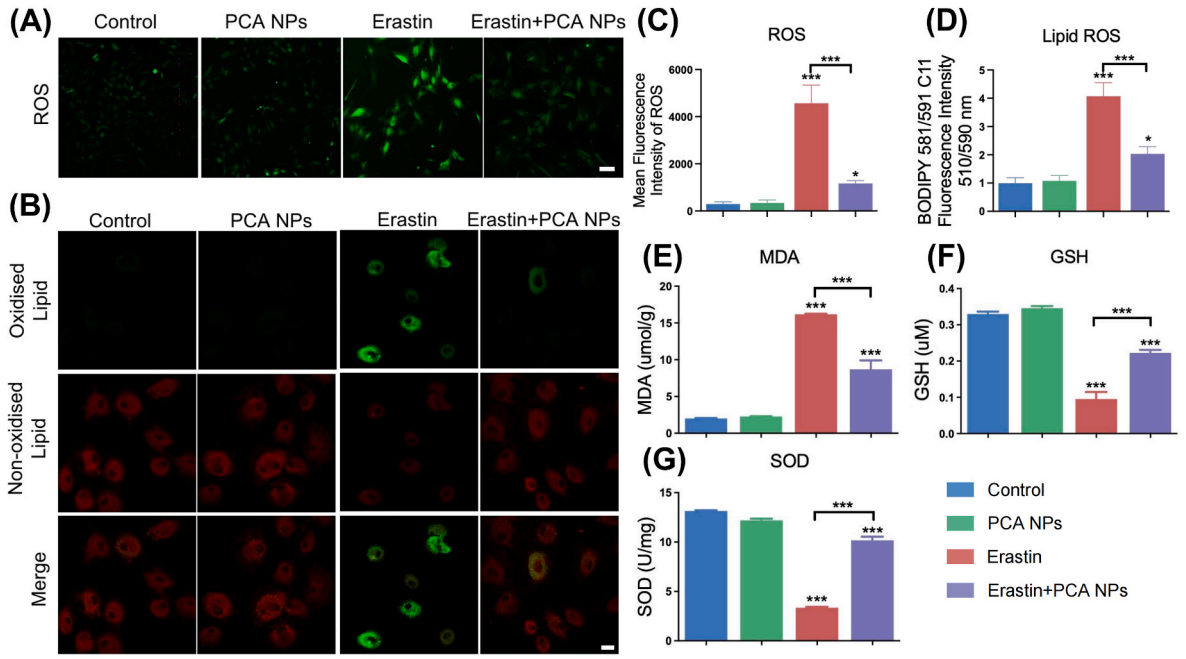

Fig. 7. PCA NPs inhibited chondrocyte lipid peroxidation induced by erastin.
(A–D) Representative fluorescence images for cellular ROS (A) and lipid ROS (B), along with their quantitative assessment via flow cytometry (C and D). Scale bar: 20 μm. (E–G) Quantitative determination of MDA (E), GSH (F), and SOD (G) Levels in cells treated with PCA NPs and stimulated with erastin. $^{*}P < 0.05$, $^{**}P < 0.01$, $^{***}P < 0.001$ in contrast to the control.

[36–39]. Oxidative pressure in the affected joint is an important factor in the evolution of TMJOA [9,40]. PCA NPs are a promising option for the treatment of TMJOA due to their effective ROS scavenging activity. The overproduction of reactive nitrogen species, including NO and ROS, commonly elevated in inflammatory conditions, is acknowledged as a cause of matrix degradation, cellular damage, mitochondrial malfunction, and alterations in protein construction in OA [41]. *p*-CA, a dietary polyphenol, has been established as an effective antioxidant, as demonstrated in previous studies. Its antioxidative properties include scavenging ABTS free radicals, DPPH free radicals, superoxide anion free radicals, and hydrogen peroxide, along with notable metal-chelating activity [42]. HA, a fundamental constituent of joint synovial fluid and cartilage matrix, is recognized for its biocompatibility and possesses both antioxidant and anti-inflammatory properties. These properties contribute to the inhibition of NO, peroxide, and hydroxyl radical production [43]. Consequently, supplementation with HA is acknowledged as a major therapeutic strategy in current OA treatment [44]. In our study, we undertook a comparative analysis of the antioxidative properties of PCA NPs and HA *in vitro*. Our findings revealed that, at a specific concentration, PCA NPs exhibited a superior antioxidant capacity compared to HA. These findings suggested that PCA NPs can potentially achieve therapeutic effects by mitigating excessive ROS generated during joint inflammation and decreasing oxidative pressure.

Nanoparticle characteristics within cartilage, including dimension, charge, and surface properties, as well as the pathological state of the joint cavity, significantly impact their pharmacokinetics. Research shows that the pore dimension within the type II collagen network of articular cartilage varies from 50 nm to 200 nm, and nanoparticles approximately 55 nm in diameter can permeate the entire cartilage construction [45–47]. However, as OA progresses, chondrocyte destruction occurs in the articular cartilage tissue, leading to a reduction in collagen and proteoglycans. Simultaneously, the porosity of the type II collagen network increases. In this context, nanoparticles demonstrate an enhanced ability to penetrate deeper into the cartilage matrix, particularly in proteoglycan-deficient cartilage compared to in normal cartilage. However, conflicting findings exist, and some studies have shown that nanoparticles with a particle dimension of 138 nm fail to penetrate damaged cartilage *in vitro*. Consequently, the established threshold for penetrating particle dimension in OA cartilage may lie between 55 nm and 140 nm [48–50]. Besides, while conventional drugs administered directly into the joint can evade lymphatic drainage, they are susceptible to swift elimination through enzymatic degradation and cellular absorption. Employing polymer nanomedical systems offers a solution by slowing down drug degradation and mitigating its effect on the joint space [50,51]. In our investigation, the particle dimension of the generated PCA NPs was approximately 118 nm, which falls within the range of the identified penetration threshold for OA cartilage. Furthermore, the dimension stability and long-term retention in the TMJ of PCA NPs are advantageous for their effective penetration and consistent functionality within OA cartilage.

Regarding the pathophysiology of TMJOA, decreased proliferation, unfavorable inflammation, reduced matrix synthesis, and catabolic matrix degradation all contribute to disease evolution [3]. Elevated local ROS levels in chondrocytes contribute to the degradation of the cartilage matrix by inhibiting matrix formation, inducing ECM breakdown, and/or reinforcing the synthesis of matrix-degrading enzymes such as MMPs and ADAMTS [52,53]. In our study, PCA NPs successfully addressed the two main pathogenic characteristics of TMJOA, namely, catabolic matrix breakdown and inflammation. This was demonstrated by decreased MMP13 and iNOS manifestation as good as increased Collagen II manifestation in rats with TMJOA-related degenerative alterations. The powerful immunosuppressive effects of *p*-CA therapy in animal models of illness are compatible with the reported suppression of inflammation and antioxidation [54,55]. Notably, we found that both the PCA NPs group and the HA group exhibited noticeable therapeutic effects at 2 and 4 weeks, while the impact on subchondral bone healing and the appearance of condylar cartilage tissue were similar in both groups. However, the therapeutic benefit of PCA NPs was greater than that of HA at 8 weeks, indicating that the effects of HA are not long-lasting, and HA can be promptly removed from the joint cavity after injection. Clinically, repeated injection are likely to lead to partial osteonecrosis of the joint tubercle and increase the possibility of bone

degeneration as a result of recurrent microtrauma, which is the main reason for the clinical limitations of its application [56]. While intra-articular HA injection can rejuvenate the rheological and viscoelastic properties of joint components, they are pivotal in affording lubrication, nutritional benefits, and anti-inflammatory effects in TMJOA management. In our study, the synthesis of PCA NPs involved the polymerization of *p*-CA monomers to form nanoparticles. Besides the anti-inflammatory and antioxidant properties exhibited by *p*-CA, the diminutive particle dimension arrangement and various features of PCA NPs led to a reduction in joint clearance rate while facilitating the continuous release of medication within the joint cavity.

To clarify the mode of action responsible for the impact of PCA NPs on TMJOA, an *in vivo* transcriptome study of TMJ condylar cartilage was carried out. The involvement of PCA NPs in chondrocytes was associated with oxidative pressure and cellular demise. Oxidative pressure and ferroptosis are intricately intertwined, with research indicating that chondrocyte ferroptosis can accelerate the onset of osteoarthritis. Ferroptosis represents a form of iron-dependent, non-apoptotic cell demise marked by an abundance of iron, lipid peroxidation, and disruptions in mitochondrial function [14,57]. Research indicates that the accelerated progress of osteoarthritis can be caused by chondrocyte ferroptosis [58–60]. As a major regulator of ferroptosis and an antioxidant enzyme, GPX4 can catalyze the reduction of lipid peroxides in the presence of GSH [61]. The dynamic equilibrium of antioxidant and peroxidation systems in cells is disrupted when lipid peroxidation ranks increase, and a crucial enzyme that encourages lipid peroxidation is ACSL4 [62,63]. In the rat model for TMJOA, the cartilage layer exhibited an upregulation in the manifestation of ACSL4 and a downregulation in GPX4, validating the connection between TMJOA injury and the suppression of antioxidant capabilities, as well as the promotion of peroxidation.

System Xc-functions as a transporter for cystine and glutamate. Within this system, SLC7A11 is a specific subunit, and when SLC7A11 is inhibited, it causes the depletion of intracellular GSH, iron-dependent lipid peroxidation, and ultimately, iron-induced cell death [64]. P53, a tumor suppressor that is essential for apoptosis, suppresses the manifestation of SLC7A11, which is essential for ferroptosis [65]. IL-1β is a widely used proinflammatory cytokine for the establishment of OA models *in vitro* [33]. IL-1β can cause chondrocyte catabolism, but it has only recently been demonstrated that IL-1β can also cause chondrocyte ferroptosis and disturb chondrocyte iron homeostasis [66]. Our research demonstrated that by inhibiting GPX4 and SLC7A11 manifestation while promoting the upregulation of ACSL4 and P53, it induces the accumulation of cellular ROS, lipid ROS, and Fe^{2+}, along with provoking mitochondrial dysfunction. These effects collectively suggest that IL-1β can subject chondrocytes to oxidative pressure, ultimately culminating in chondrocyte ferroptosis. These findings suggest that IL-1β might serve as a link between inflammation and chondrocyte ferroptosis in TMJOA.

Activating the GPX4 pathway or lowering lipid peroxidation are two ways in which several naturally occurring compounds with antioxidant or anti-inflammatory properties, such as D-mannose, stigmasterol, and icariin, reduce ferroptosis. This slows the deterioration of cartilage and the evolution of osteoarthritis [67]. Our studies showed that PCA NPs slowed the course of TMJOA and prevented chondrocyte ferroptosis. We first surveied increased GPX4 manifestation and decreased ACSL4 manifestation in the cartilage layer of the TMJOA model rats treated with PCA NPs. Furthermore, we substantiated that PCA NPs had a positive impact on the mitochondrial architecture, reinstating the mitochondrial membrane potential. Simultaneously, they significantly elevated the ranks of GPX4 and SLC7A11 manifestation while decreasing cellular ROS and lipid-associated ROS generation, P53, ACSL4, MDA manifestation, and Fe^{2+} accumulation in chondrocytes subjected to erastin and IL-1β stimulation. The evidence points to the fact that PCA NPs may be pivotal for preventing ferroptosis in both *in vivo* and *in vitro* contexts of TMJOA.

5. Conclusion

In conclusion, we have introduced PCA NPs, a dual-function nanoparticle with antioxidant and anti-inflammatory properties, for treating TMJOA. Our study outcomes underscore the preventative advantages of PCA NPs in addressing TMJOA, as demonstrated through a combination of *in vitro* and *in vivo* experiments. Remarkably, PCA NPs exhibited the capacity to decelerate the advancement of TMJOA by suppressing chondrocyte ferroptosis induced by erastin and IL-1β stimulation. In summary, PCA NPs mitigate the course of TMJOA and facilitate TMJ repair and regeneration by initiating a well-coordinated response of suppressing inflammation and oxidative stress, increasing proliferation and matrix production, and inhibiting chondrocyte ferroptosis and matrix decomposition (Scheme 1). Therefore, PCA NPs have emerged as a promising disease-modifying therapy for individuals with TMJOA.

Ethics approval and consent to participate

The study protocol and experimental procedures involving animal subjects were reviewed and approved by the Sun Yat-Sen University Institutional Animal Care and Use Committee (Approval Number: SYSU-IACUC-2022-000275). Appropriate measures were taken to minimize any potential suffering or harm, following the ethical guidelines for animal research.

Data availability statement

The data that support the findings of this study are available from the corresponding author upon reasonable request.

CRediT authorship contribution statement

Jiaxin Guo: Writing – original draft, Visualization, Validation, Software, Methodology, Formal analysis, Data curation, Conceptualization. **Kai Su:** Writing – original draft, Visualization, Validation, Software, Methodology, Formal analysis, Data curation, Conceptualization. **Liying Wang:** Writing – original draft, Visualization, Software, Methodology, Funding acquisition, Formal analysis, Data curation, Conceptualization. **Bingyu Feng:** Writing – original draft, Visualization, Validation, Software, Methodology, Formal analysis, Data curation, Conceptualization. **Xinru You:** Software, Methodology, Data curation. **Miao Deng:** Software, Methodology, Data curation. **Wei Seong Toh:** Writing – review & editing. **Jun Wu:** Writing – review & editing, Validation, Supervision, Project administration, Funding acquisition. **Bin Cheng:** Writing – review & editing, Validation, Supervision, Project administration, Funding acquisition. **Juan Xia:** Writing – review & editing, Validation, Supervision, Project administration, Funding acquisition.

Declaration of competing interest

The authors declare that they have no known competing financial interests or personal relationships that could have appeared to influence the work reported in this paper.

Acknowledgements

This study was supported by grants from the National Natural Science Foundation of China (Grant No. 82170960 and No. 52173150), the Science and Technology Program of Guangzhou, China (Grant No. 202206080009), Guangzhou Science and Technology Program City-University Joint Funding Project (Grant No. 2023A03J0001) and China Postdoctoral Science Foundation (Grant No. 2022M723670).

Appendix A. Supplementary data

Supplementary data to this article can be found online at https://doi.org/10.1016/j.bioactmat.2024.06.007.

References

[1] J.G. Quicke, P.G. Conaghan, N. Corp, G. Peat, Osteoarthritis year in review 2021: epidemiology & therapy, Osteoarthritis Cartilage 30 (2) (2022) 196–206.
[2] Q. Yao, X. Wu, C. Tao, W. Gong, M. Chen, M. Qu, Y. Zhong, T. He, S. Chen, G. Xiao, Osteoarthritis: pathogenic signaling pathways and therapeutic targets, Signal Transduct. Targeted Ther. 8 (1) (2023) 56.
[3] A. Hill, J. Duran, P. Purcell, Lubricin protects the temporomandibular joint surfaces from degeneration, PLoS One 9 (9) (2014) e106497.
[4] X.D. Wang, J.N. Zhang, Y.H. Gan, Y.H. Zhou, Current understanding of pathogenesis and treatment of TMJ osteoarthritis, J. Dent. Res. 94 (5) (2015) 666–673.
[5] F. Barry, F. Chai, H. Chijcheapaza-Flores, M.J. Garcia-Fernandez, N. Blanchemain, R. Nicot, Systematic review of studies on drug-delivery systems for management of temporomandibular-joint osteoarthritis, J Stomatol Oral Maxillofac Surg 123 (5) (2022) e336–e341.
[6] W. Li, S. Wu, L. Ren, B. Feng, Z. Chen, Z. Li, B. Cheng, J. Xia, Development of an antiswelling hydrogel system incorporating M2-exosomes and photothermal effect for diabetic wound healing, ACS Nano 17 (21) (2023) 22106–22120.
[7] F. Liu, A. Steinkeler, Epidemiology, diagnosis, and treatment of temporomandibular disorders, Dent Clin North Am 57 (3) (2013) 465–479.
[8] J.A. Bolduc, J.A. Collins, R.F. Loeser, Reactive oxygen species, aging and articular cartilage homeostasis, Free Radic. Biol. Med. 132 (2019) 73–82.
[9] L. Xiong, H. Bao, S. Li, D. Gu, Y. Li, Q. Yin, W. Li, L. Miao, C. Liu, Cerium oxide nanoparticles protect against chondrocytes and cartilage explants from oxidative stress via Nrf2/HO-1 pathway in temporomandibular joint osteoarthritis, Front. Bioeng. Biotechnol. 11 (2023) 1076240.
[10] X. Huang, X. Pan, X. Xiong, Z. Zhao, X. Cen, Drug delivery systems for treatment of temporomandibular joint osteoarthritis, Front. Pharmacol. 13 (2022) 1054703.
[11] R. Barnett, Osteoarthritis, Lancet 391 (10134) (2018) 1985.
[12] E. Charlier, B. Relic, C. Deroyer, O. Malaise, S. Neuville, J. Collee, M.G. Malaise, D. De Seny, Insights on molecular mechanisms of chondrocytes death in osteoarthritis, Int. J. Mol. Sci. 17 (12) (2016) 2146.
[13] H. Yang, Y. Wen, M. Zhang, Q. Liu, H. Zhang, J. Zhang, L. Lu, T. Ye, X. Bai, G. Xiao, M. Wang, MTORC1 coordinates the autophagy and apoptosis signaling in articular chondrocytes in osteoarthritic temporomandibular joint, Autophagy 16 (2) (2020) 271–288.
[14] X. Yao, K. Sun, S. Yu, J. Luo, J. Guo, J. Lin, G. Wang, Z. Guo, Y. Ye, F. Guo, Chondrocyte ferroptosis contribute to the progression of osteoarthritis, J Orthop Translat 27 (2021) 33–43.
[15] X. Jiang, B.R. Stockwell, M. Conrad, Ferroptosis: mechanisms, biology and role in disease, Nat. Rev. Mol. Cell Biol. 22 (4) (2021) 266–282.
[16] D. Tang, X. Chen, R. Kang, G. Kroemer, Ferroptosis: molecular mechanisms and health implications, Cell Res. 31 (2) (2021) 107–125.
[17] S. Zhang, J. Xu, H. Si, Y. Wu, S. Zhou, B. Shen, The role played by ferroptosis in osteoarthritis: evidence based on iron dyshomeostasis and lipid peroxidation, Antioxidants 11 (9) (2022) 1668.
[18] Z. Guo, J. Lin, K. Sun, J. Guo, X. Yao, G. Wang, L. Hou, J. Xu, J. Guo, F. Guo, Deferoxamine alleviates osteoarthritis by inhibiting chondrocyte ferroptosis and activating the Nrf2 pathway, Front. Pharmacol. 13 (2022) 791376.
[19] P. Dulbecco, V. Savarino, Therapeutic potential of curcumin in digestive diseases, World J. Gastroenterol. 19 (48) (2013) 9256–9270.
[20] B. Ren, M.X. Kwah, C. Liu, Z. Ma, M.K. Shanmugam, L. Ding, X. Xiang, P.C. Ho, L. Wang, P.S. Ong, B.C. Goh, Resveratrol for cancer therapy: challenges and future perspectives, Cancer Lett. 515 (2021) 63–72.
[21] L. Li, S. Sun, L. Tan, Y. Wang, L. Wang, Z. Zhang, L. Zhang, Polystyrene nanoparticles reduced ROS and inhibited ferroptosis by triggering lysosome stress and TFEB nucleus translocation in a size-dependent manner, Nano Lett. 19 (11) (2019) 7781–7792.
[22] Y.C. Boo, p-Coumaric acid as an active ingredient in cosmetics: a review focusing on its antimelanogenic effects, Antioxidants 8 (8) (2019) 275.
[23] G. Bhattarai, C.K. Min, Y.M. Jeon, R. Bashyal, S.B. Poudel, S.H. Kook, J.C. Lee, Oral supplementation with p-coumaric acid protects mice against diabetes-associated spontaneous destruction of periodontal tissue, J. Periodontal. Res. 54 (6) (2019) 690–701.
[24] A. Abdel-Moneim, A.I. Yousef, S.M. Abd El-Twab, E.S. Abdel Reheim, M.B. Ashour, Gallic acid and *p*-coumaric acid attenuate type 2 diabetes-induced neurodegeneration in rats, Metab. Brain Dis. 32 (4) (2017) 1279–1286.
[25] X. Huang, Y. You, Y. Xi, B. Ni, X. Chu, R. Zhang, H. You, p-Coumaric acid attenuates IL-1beta-induced inflammatory responses and cellular senescence in rat chondrocytes, Inflammation 43 (2) (2020) 619–628.
[26] T.E. Kavanaugh, T.A. Werfel, H. Cho, K.A. Hasty, C.L. Duvall, Particle-based technologies for osteoarthritis detection and therapy, Drug Deliv Transl Res 6 (2) (2016) 132–147.
[27] X.R. You, L.Y. Wang, L. Wang, J. Wu, Rebirth of aspirin synthesis by-product: prickly poly(salicylic acid) nanoparticles as self-anticancer drug carrier, Adv. Funct. Mater. 31 (33) (2021) 2100805.
[28] K.Y. Ou, X.J. Xu, S.Y. Guan, R.H. Zhang, X.Y. Zhang, Y. Kang, J. Wu, Nanodrug carrier based on poly(ursolic acid) with self-anticancer activity against colorectal cancer, Adv. Funct. Mater. 30 (9) (2020) 1907857.
[29] Y.H. Zheng, X.R. You, S.Y. Guan, J. Huang, L.Y. Wang, J.Y. Zhang, J. Wu, Poly (Ferulic acid) with an anticancer effect as a drug nanocarrier for enhanced colon cancer therapy, Adv. Funct. Mater. 29 (15) (2019) 1808646.
[30] L.Y. Wang, X.R. You, C.L. Dai, Y.F. Fang, J. Wu, Development of poly(p-coumaric acid) as a self-anticancer nanocarrier for efficient and biosafe cancer therapy, Biomater Sci-Uk 10 (9) (2022) 2263–2274.
[31] X.D. Wang, X.X. Kou, D.Q. He, M.M. Zeng, Z. Meng, R.Y. Bi, Y. Liu, J.N. Zhang, Y. H. Gan, Y.H. Zhou, Progression of cartilage degradation, bone resorption and pain in rat temporomandibular joint osteoarthritis induced by injection of iodoacetate, PLoS One 7 (9) (2012) e45036.
[32] W.C. Chu, S. Zhang, T.J. Sng, Y.J. Ong, W.-L. Tan, V.Y. Ang, C.B. Foldager, W. S. Toh, Distribution of pericellular matrix molecules in the temporomandibular joint and their chondroprotective effects against inflammation, Int. J. Oral Sci. 9 (1) (2017) 43–52.
[33] S. Zhang, K.Y.W. Teo, S.J. Chuah, R.C. Lai, S.K. Lim, W.S. Toh, MSC exosomes alleviate temporomandibular joint osteoarthritis by attenuating inflammation and restoring matrix homeostasis, Biomaterials 200 (2019) 35–47.
[34] N. Li, W. Wang, H. Zhou, Q.Q. Wu, M.X. Duan, C. Liu, H.M. Wu, W. Deng, D. F. Shen, Q.Z. Tang, Ferritinophagy-mediated ferroptosis is involved in sepsis-induced cardiac injury, Free Radical Bio Med 160 (2020) 303–318.
[35] X. Chen, R. Kang, G. Kroemer, D. Tang, Organelle-specific regulation of ferroptosis, Cell Death Differ. 28 (10) (2021) 2843–2856.
[36] S.M. Shaffer, J.M. Brismee, P.S. Sizer, C.A. Courtney, Temporomandibular disorders. Part 1: anatomy and examination/diagnosis, J. Man. Manip. Ther. 22 (1) (2014) 2–12.
[37] J.L. Sun, J.F. Yan, S.B. Yu, J. Zhao, Q.Q. Lin, K. Jiao, MicroRNA-29b promotes subchondral bone loss in TMJ osteoarthritis, J. Dent. Res. 99 (13) (2020) 1469–1477.
[38] J. Yan, M. Shen, B. Sui, W. Lu, X. Han, Q. Wan, Y. Liu, J. Kang, W. Qin, Z. Zhang, D. Chen, Y. Cao, S. Ying, F.R. Tay, L.N. Niu, K. Jiao, Autophagic LC3(+) calcified extracellular vesicles initiate cartilage calcification in osteoarthritis, Sci. Adv. 8 (19) (2022) eabn1556.
[39] J.F. Yan, W.P. Qin, B.C. Xiao, Q.Q. Wan, F.R. Tay, L.N. Niu, K. Jiao, Pathological calcification in osteoarthritis: an outcome or a disease initiator? Biol. Rev. 95 (4) (2020) 960–985.
[40] Z. Zhang, L. Yuan, Y. Liu, R. Wang, Y. Zhang, Y. Yang, H. Wei, J. Ma, Integrated cascade nanozyme remodels chondrocyte inflammatory microenvironment in temporomandibular joint osteoarthritis via inhibiting ROS-NF-kappaB and MAPK pathways, Adv. Healthcare Mater. 12 (10) (2023) e2203195.
[41] R.C. Gupta, R. Lall, A. Srivastava, A. Sinha, Hyaluronic acid: molecular mechanisms and therapeutic trajectory, Front. Vet. Sci. 6 (2019) 192.
[42] I. Kilic, Y. Yesiloglu, Spectroscopic studies on the antioxidant activity of p-coumaric acid, Spectrochim. Acta Mol. Biomol. Spectrosc. 115 (2013) 719–724.
[43] W.K.V. Paiva, W. Medeiros, C.F. Assis, E.S. Dos Santos, F.C. de Sousa Junior, Physicochemical characterization and *in vitro* antioxidant activity of hyaluronic acid produced by Streptococcus zooepidemicus CCT 7546, Prep. Biochem. Biotechnol. 52 (2) (2022) 234–243.
[44] J. Dulinska-Litewka, K. Dykas, D. Felkle, K. Karnas, G. Khachatryan, A. Karewicz, Hyaluronic acid-silver nanocomposites and their biomedical applications, A Review, Materials (Basel) 15 (1) (2021) 234.
[45] C. Sacchetti, R. Liu-Bryan, A. Magrini, N. Rosato, N. Bottini, M. Bottini, Polyethylene-glycol-modified single-walled carbon nanotubes for intra-articular delivery to chondrocytes, ACS Nano 8 (12) (2014) 12280–12291.
[46] C.D. DiDomenico, M. Lintz, L.J. Bonassar, Molecular transport in articular cartilage - what have we learned from the past 50 years? Nat. Rev. Rheumatol. 14 (7) (2018) 393–403.
[47] H. Yan, X. Duan, H. Pan, N. Holguin, M.F. Rai, A. Akk, L.E. Springer, S.A. Wickline, L.J. Sandell, C.T. Pham, Suppression of NF-kappaB activity via nanoparticle-based siRNA delivery alters early cartilage responses to injury, Proc. Natl. Acad. Sci. U.S. A. 113 (41) (2016) E6199–E6208.
[48] K.A. Elsaid, L. Ferreira, T. Truong, A. Liang, J. Machan, G.G. D'Souza, Pharmaceutical nanocarrier association with chondrocytes and cartilage explants: influence of surface modification and extracellular matrix depletion, Osteoarthritis Cartilage 21 (2) (2013) 377–384.
[49] X. Li, B. Dai, J. Guo, L. Zheng, Q. Guo, J. Peng, J. Xu, L. Qin, Nanoparticle-cartilage interaction: pathology-based intra-articular drug delivery for osteoarthritis therapy, Nano-Micro Lett. 13 (1) (2021) 149.
[50] S. Brown, S. Kumar, B. Sharma, Intra-articular targeting of nanomaterials for the treatment of osteoarthritis, Acta Biomater. 93 (2019) 239–257.
[51] M.A. Tryfonidou, G. de Vries, W.E. Hennink, L.B. Creemers, "Old Drugs, New Tricks" - local controlled drug release systems for treatment of degenerative joint disease, Adv. Drug Deliv. Rev. 160 (2020) 170–185.
[52] K. Sun, J. Luo, X. Jing, W. Xiang, J. Guo, X. Yao, S. Liang, F. Guo, T. Xu, Hyperoside ameliorates the progression of osteoarthritis: an *in vitro* and *in vivo* study, Phytomedicine 80 (2021) 153387.
[53] X. Pan, T. Chen, Z. Zhang, X. Chen, C. Chen, L. Chen, X. Wang, X. Ying, Activation of Nrf2/HO-1 signal with Myricetin for attenuating ECM degradation in human chondrocytes and ameliorating the murine osteoarthritis, Int. Immunopharm. 75 (2019) 105742.
[54] Y.H. Li, Q. He, Y.Z. Chen, Y.F. Du, Y.X. Guo, J.Y. Xu, L.Q. Qin, p-Coumaric acid ameliorates ionizing radiation-induced intestinal injury through modulation of oxidative stress and pyroptosis, Life Sci. 278 (2021) 119546.

[55] S.J. Pragasam, V. Venkatesan, M. Rasool, Immunomodulatory and anti-inflammatory effect of p-coumaric acid, a common dietary polyphenol on experimental inflammation in rats, Inflammation 36 (1) (2013) 169–176.
[56] N. Ferreira, D. Masterson, R. Lopes de Lima, B. de Souza Moura, A.T. Oliveira, T. Kelly da Silva Fidalgo, A.C.P. Carvalho, M.F. DosSantos, E. Grossmann, Efficacy of viscosupplementation with hyaluronic acid in temporomandibular disorders: a systematic review, J. Cranio-Maxillo-Fac. Surg. 46 (11) (2018) 1943–1952.
[57] J.X. Ren, C. Li, X.L. Yan, Y. Qu, Y. Yang, Z.N. Guo, Crosstalk between oxidative stress and ferroptosis/oxytosis in ischemic stroke: possible targets and molecular mechanisms, Oxid. Med. Cell. Longev. 2021 (2021) 6643382.
[58] X. Jing, J. Lin, T. Du, Z. Jiang, T. Li, G. Wang, X. Liu, X. Cui, K. Sun, Iron overload is associated with accelerated progression of osteoarthritis: the role of DMT1 mediated iron homeostasis, Front. Cell Dev. Biol. 8 (2020) 594509.
[59] A. Ioan-Facsinay, M. Kloppenburg, Bioactive lipids in osteoarthritis: risk or benefit? Curr. Opin. Rheumatol. 30 (1) (2018) 108–113.
[60] R.S. Lane, Y. Fu, S. Matsuzaki, M. Kinter, K.M. Humphries, T.M. Griffin, Mitochondrial respiration and redox coupling in articular chondrocytes, Arthritis Res. Ther. 17 (1) (2015) 54.
[61] T.M. Seibt, B. Proneth, M. Conrad, Role of GPX4 in ferroptosis and its pharmacological implication, Free Radic. Biol. Med. 133 (2019) 144–152.
[62] M. Maiorino, M. Conrad, F. Ursini Gpx4, Lipid peroxidation, and cell death: discoveries, rediscoveries, and open issues, Antioxidants Redox Signal. 29 (1) (2018) 61–74.
[63] S. Doll, B. Proneth, Y.Y. Tyurina, E. Panzilius, S. Kobayashi, I. Ingold, M. Irmler, J. Beckers, M. Aichler, A. Walch, H. Prokisch, D. Trumbach, G. Mao, F. Qu, H. Bayir, J. Fullekrug, C.H. Scheel, W. Wurst, J.A. Schick, V.E. Kagan, J.P. Angeli, M. Conrad, ACSL4 dictates ferroptosis sensitivity by shaping cellular lipid composition, Nat. Chem. Biol. 13 (1) (2017) 91–98.
[64] J.Y. Cao, S.J. Dixon, Mechanisms of ferroptosis, Cell. Mol. Life Sci. 73 (11–12) (2016) 2195–2209.
[65] R. Kang, G. Kroemer, D. Tang, The tumor suppressor protein p53 and the ferroptosis network, Free Radic. Biol. Med. 133 (2019) 162–168.
[66] L. Deng, S. He, N. Guo, W. Tian, W. Zhang, L. Luo, Molecular mechanisms of ferroptosis and relevance to inflammation, Inflamm. Res. 72 (2) (2023) 281–299.
[67] Q. Ru, Y. Li, W. Xie, Y. Ding, L. Chen, G. Xu, Y. Wu, F. Wang, Fighting age-related orthopedic diseases: focusing on ferroptosis, Bone Res 11 (1) (2023) 12.